Biosensors and Bioelectronics 32 (2012) 69–75

Contents lists available at SciVerse ScienceDirect

Biosensors and Bioelectronics

journal homepage: www.elsevier.com/locate/bios

Rapid, sensitive and label-free detection of Shiga-toxin producing *Escherichia coli* O157 using carbon nanotube biosensors

Sowmya Subramanian, Konrad H. Aschenbach, Jennifer P. Evangelista, Mohamed Badaoui Najjar, Wenxia Song, Romel D. Gomez *

University of Maryland, College Park, MD 20742, United States

ARTICLE INFO

Article history:
Received 30 September 2011
Received in revised form
15 November 2011
Accepted 18 November 2011
Available online 2 December 2011

Keywords:
Biosensor
Deoxyribonucleic acid (DNA)
E. coli
Field-effect transistor (FET)
Carbon nanotube (CNT)

ABSTRACT

An electronic platform to detect very small amounts of genomic DNA from bacteria without the need for PCR amplification and molecular labeling is described. The system uses carbon nanotube field-effect transistor (FET) arrays whose electrical properties are affected by minute electrical charges localized on their active regions. Two pathogenic strains of *E. coli* are used to evaluate the detection properties of the transistor arrays. Described herein are the results for detection of synthetic oligomers, unpurified and highly purified genomic DNA at various concentrations and their comparison against non-specific binding. In particular, the capture of genomic DNA of *E. coli* O157:H7 by a specific oligonucleotide probe coated onto the transistor array results in a significant shift in the threshold (gate-source) voltage (V_{th}). By contrast the signal under the same procedure using a different strain, *E. coli* O45 that is non-complementary to the probe remained nearly constant. This work highlights the detection sensitivity and efficacy of this biosensor without stringent requirement for DNA sample preparation.

1. Introduction

Food borne illnesses are a growing cause of concern in the USA and worldwide. The yearly incidences of food-borne illnesses are estimated to be about 81 million cases just in the USA, of which 91% of the total outbreaks are associated with bacteria (Beran et al., 1991; Potter et al., 1997). *E. coli* O157:H7 is considered to be one the most dangerous food borne pathogens (Griffin and Tauxe, 1991; Buchanan and Doly, 1997). This strain produces large quantities of a potent toxin that can cause hemorrhagic colitis or hemolytic uremic syndrome which may lead to death (Quadri and Kayali, 1998; Jaeger and Acheson, 2000; Ivnitski et al., 1999). In North America, *E. coli* O157:H7 has been implicated as the major cause of hemolytic uremic syndrome (85–95%). A similar strain the *E. coli* O104 has caused an outbreak in Europe in June 2011 that has left at least 22 dead, thousands sickened and nearly $600 M per week in lost agricultural revenue (Associated Press, 2011).

Early detection of this pathogen in food production from farm to table (Ivnitski et al., 1999) is key in minimizing its spread and arresting potential outbreaks. The traditional methods for the detection of bacteria involve a series of steps: pre-enrichment, selective enrichment, biochemical screening and serological confirmation (Helrich, 1990; Kaspar and Tartera, 1990; Tietjen and Fung, 1995; Hobson et al., 1996). The steps are labor-intensive, time-consuming tests and require specialized expensive equipment and trained personnel. For example recent detection methods use polymerase chain reaction (PCR) that is very sensitive but require purified DNA samples, hours of processing and considerable bio-molecular expertise (Meng et al., 1996; Sperveslage et al., 1996) for confirmed identification to be made. Such a process could take 48 h to about 5 days (Karch et al., 1999) to complete. Additionally, transportation of the specimen to reference state labs causes additional delays, which further extends the confirmation time from a few days to a few weeks in some cases. Therefore, there is a clear and present need for rapid, simple and sensitive identification techniques that could be deployed in the field with minimal sophisticated instrumentation. In this paper, a method for electronic label-free sensing of *E. coli* specific pathogenic DNA is reported that addresses this need. A proof of concept is presented which shows specific detection of minute amounts of *E. coli* O157:H7 DNA extracted from highly purified samples and also crude *E. coli* O157:H7 DNA extracted by the boiling method. Detection is on the order of picomoles quantities within several hours and is compared against non-specific binding.

2. Materials and methods

2.1. Design of the carbon nanotube field-effect transistor

The central component of the system is a large array of carbon nanotube field-effect transistors (CNTFETs) (Pandana et al., 2008).

* Corresponding author at: University of Maryland, 2313 A.V. Williams Building, Department of Electrical and Computer Engineering, College Park, MD 20742, United States. Tel.: +1 301 405 7755.
E-mail address: rdgomez@umd.edu (R.D. Gomez).

0956-5663/$ – see front matter © 2011 Elsevier B.V. All rights reserved.
doi:10.1016/j.bios.2011.11.040

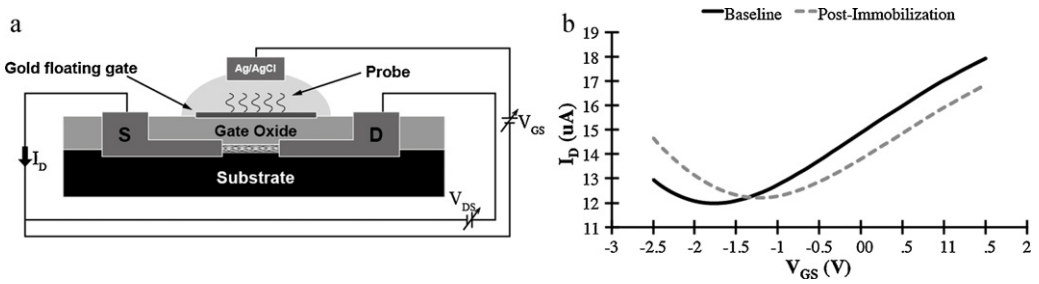

Fig. 1. (a) Principle of operation. When target DNA is captured at the gold floating gate, the curve representing the drain-source current (I_D) versus gate voltage (V_{GS}) shifts by an amount, ΔV_{th}, commensurate with the amount of extra charges that have been captured. (b) Typical $I_{DS} - V_{GS}$ to show baseline (solid) and post-immobilization (dashed). Post-immobilization refers to the measurement after the probe has attached to the gold using thiol–gold chemistry. Au–Cr films are patterned to form S and D electrodes.

Briefly, each transistor is comprised of carbon nanotubes grown on 500 μm thick silicon oxide substrate and contacted by two electrodes labeled source (S) and drain (D). A schematic diagram is shown in Fig. 1a. The nanotubes are covered by a thin layer of high quality oxide material, with thickness between 30 and 60 nm which electrically insulates and prevents liquids from making direct electrical contact with the carbon nanotubes. A segment of the oxide directly on top the carbon nanotubes is designated as the active area, and coated with gold. It becomes the repository of single stranded probe and target DNA charges that will ultimately be detected. The sensing strategy relies on the fact that the DNA is intrinsically charged from its phosphate backbone. A voltage applied between the drain and source, V_{DS}, provides the bias to push the electrons across the carbon nanotubes creating a drain current, I_D. The voltage, V_{GS}, applied between the Ag–AgCl electrode immersed in the liquid buffer and the source, provides a gate potential to increase (or decrease) the current of the carbon nanotube transistors by modulating the number of mobile charges on the carbon nanotubes. For small V_{DS} (~100 mV), the current I_D versus V_{GS} has the generic form shown in Fig. 1b. The typical leakage current between gate and source is on the order of a few pico amperes. The value of the voltage V_{GS} at minimum current is called V_{th} or threshold voltage for conduction. When additional charges accumulate at the oxide surface, e.g. due to capture of target DNA, the electric field from these charges shifts the threshold voltage. Under the conditions in this study, the voltage shift has a simple relation with the bound surface charges given by,

$$\Delta V_{th} = \frac{\Delta \sigma_{DNA}}{C_D} \quad (1)$$

where $\Delta\sigma_{DNA}$ is the added surface charge per unit area on the transistor and C_D is the effective capacitance per unit area arising from the double layer the screening effect of the mobile ions around the bound charges. C_D is given by

$$C_D = \frac{\varepsilon_{buffer}}{\lambda_{Debye}} \quad (2)$$

where λ_{Debye} is the Debye length and ε_{buffer} is approximately $80\varepsilon_0$, the permittivity for water. The phenomenon described by Eq. (1) is exploited for the detection of complementary DNA–DNA binding by tethering an oligonucleotide probe whose sequence is complementary to a target DNA or RNA. The singly ionized phosphate backbone of the nucleic acid strands gives rise to charges. Thus, in the process of Watson–Crick base pairing the target DNA captured by the probe is concommitant to an increase the surface charge density which results in the voltage shift given in Eq. (1).

Fig. 2a shows the sensor chip and the platform. The chip is mounted on a removable carrier with appropriate wire-bonding. A reservoir for liquid buffer containment is made from cut polypropylene tube and mounted on the chip. It can accommodate up to 100 μl. A Ag–AgCl electrode is kept in contact with the buffer from the top of the liquid reservoir during measurement. The Ag–AgCl electrode is attached to a plastic lid which facilitates the alignment of the electrode inside the reservoir. The measurement is automated with the aid of two multiplexers that allow each transistor to be scanned. The optical micrograph shown in Fig. 2b identifies the placement of the transistors and the electrical connections that bring the signal from the active areas in the interior to the contact pads (not shown) at the edges of the die. Fig. 2c is a scanning electron micrograph of the active areas of the devices. The dark contrast region are the metal pattern, the intermediate contrast (green) region are the semiconductor with oxide passivation layer and the bright region (gold) are the gold coated gate active areas upon which the gold oligomers are immobilized. Six complete transistors are shown in this figure, which are connected by a single source electrode running through the center. The six horizontal lines that terminate into rectangular patterns are the individual drain electrodes. The dashed line indicates the overlap with the Au gate active areas. The separation between the source and drain contacts for each transistor is 15 μm. The carbon nanotubes underneath are in the form of a mesh. The CNTs are the conduction channels that function very similar to the depletion layer of a conventional MOSFET. Based upon the drain current we estimate approximately 10 carbon nanotubes channels contribute that to the conductance. A systems level block diagram is shown in Fig. 2d. With the source and gate voltages common to all transistors, the multiplexer unit selects each transistor one after another through the drain electrodes. For every transistor, the I_D is measured as the V_{GS} is swept from $-V_o$ to $+V_o$ (V_o typically 1.5 V).

Other groups, have used similar techniques, to demonstrate detection of DNA binding as applied to 30-mer ssDNA and 21-mer ssDNA target oligomers, respectively (Star et al., 2007; Maehashi et al., 2004). The present device differs from the earlier implementations by having oxide encapsulation of the CNTs sensors, incorporation of gold-coated active areas and gating through the oxide. By encapsulating the CNTs with oxide, they become isolated from the chemical environment, which reduces spurious signals from nonspecific binding of molecules to the CNT walls and thus minimizing false positives. Furthermore by using Au as the gate surface, a standard thiol chemistry protocol for probe immobilization can be used. A new 45-mer probe specific to *E. coli* O157:H7 was developed in this work along with the protocols for immobilization, hybridization, dehybridization and blanking that are essential for the proper operation and accurate analysis of results.

2.2. DNA immobilization

The thiol modified DNA probes were synthesized by Integrated DNA Technologies. The probes were HPLC purified and lyophilized. They were resuspended in Top Gate Buffer (TGB) (1 mM TE pH 8.0, diluted to 0.1× via Ultra Pure Water). The probes were DTT treated to cleave the disulphide bond and create a free sulphide needed to covalently attach to the Gold Attachment Surface (GAS) of the

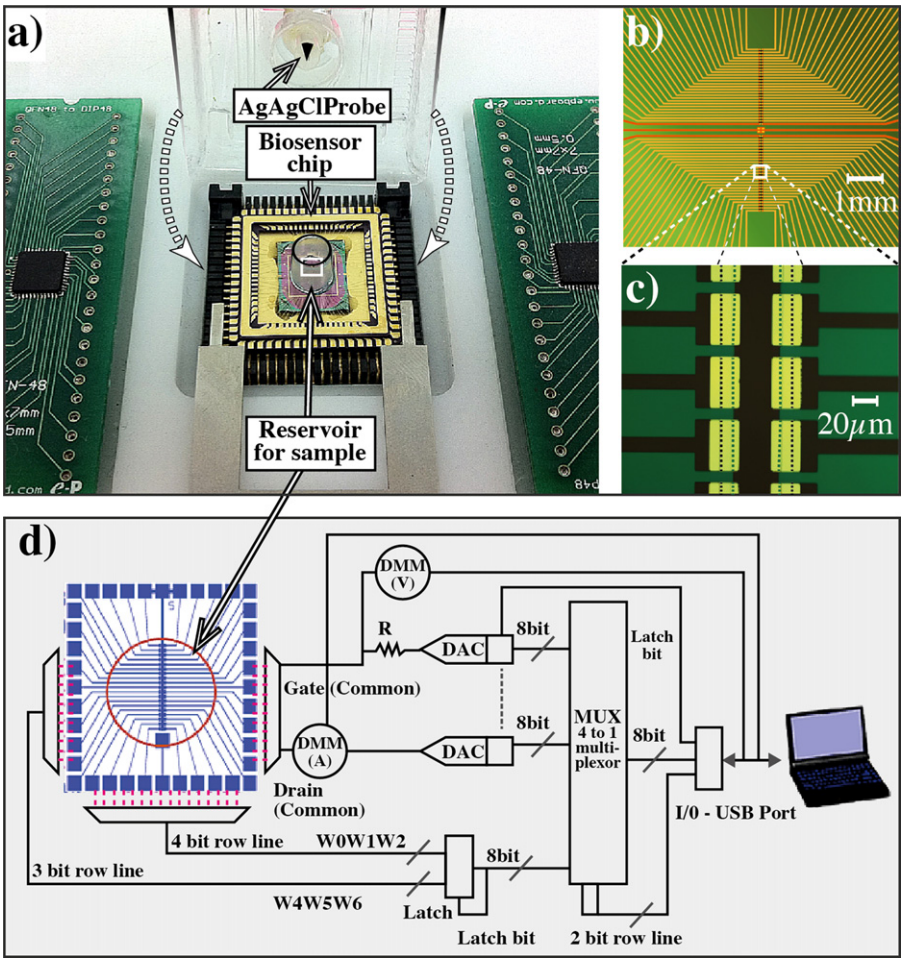

Fig. 2. (a) The sensor chip seen under 1 x magnification. (b) Higher resolution optical micrograph of the transistor array. (c) SEM of the active areas (GAS). (d) The system level block diagram of the biosensor.

transistors. The DTT treated probes were aliquoted and stored at −4 °C. The concentration of the probes was determined using Nanodrop®.

The DNA probe solution was heated to 55 °C for 2 min prior to immobilizing on the GAS. The GAS's were rinsed by manual pipetting of TGB 3 times and followed by blow-drying prior to spotting with the probe. For probe immobilization on the CNTFET, the chips were soaked in 25 μl of the probe solution overnight in a humidified chamber at room temperature, which was followed by a washing procedure (using TGB) to remove excess and unbound DNA probes. Initial experiments used mercapto-hexanol as a blocking agent but it was discovered to be unnecessary.

2.3. DNA hybridization

The target DNA was diluted to the required concentration using 100 mM NaCl in TGB. This DNA solution was denatured at 95 °C for 2 minutes and snap cooled to 55 °C. Hybridization mixture of 100 mM NaCl in TGB and *E. coli* target DNA was then applied to the device and incubated for 30 min at 55 °C in a humid chamber. Post-hybridization wash was performed by rinsing with heated TGB at 55 °C three times followed by a rinsing with room temperature TGB three times. Device was then allowed to cool down to room temperature for 2 min before placing on the platform for measurement. Blank hybridizations were also performed with just 100 mM NaCl in TGB (without DNA) to test for background signal/device stability.

2.4. DNA samples and their sequences

The immobilization was followed by hybridization with various DNA targets. Synthetic oligonucleotides, PCR amplified DNA fragments, genomic DNA isolated using the UltraClean Microbial DNA Isolation Kit (MO BIO Laboratories, Inc.) and crude DNA extracted by the boiling method were used at various concentrations to derive a dose response. The sequences of the probe, complementary synthetic target and non-complementary negative control used are listed in Table 1.

A 45-mer probe was designed specifically for the *E. coli* O157:H7 strain using Visual OMP™ Nucleic Acid Software. The probe was designed to target the O-antigen which is present on the outer membrane of *E. coli* that determines the serogroup of the bacteria. There are 186 O-antigens documented in the *E. coli* typing schemes and these have very low levels of similarity with other species (Samuel and Reeves, 2003). The target gene wzy, located in the O-antigen gene cluster encodes genes responsible for the synthesis of the O-antigen. The wzy (O-antigen polymerase) gene is highly variable among the different *E. coli* serogroups and is commonly used to develop serotype-specific assays (Liu and Fratamico, 2006).

Table 1
Synthetic nucleotide sequences.

Name	Sequence
E. coli O157 Probe-45 mer	/5ThioMC6-D//iSp9/GTT GTT TTA TCT AAG TTT AGG ACA AGA CGG AGA ACA AAA TGA CTC
E. coli O157 target	5′-GAG TCA TTT TGT TCT CCG TCT TGT CCT AAA CTT AGA TAA AAC AAC-3′
E. coli O45 target (negative control)	5′-AAC TAT CCC ATG ATA TGT CGG TAT ACC GAA CTC GGT ATA ATT ATA-3′

The 45-mer probe was developed to target the wzy gene (GenBank: AF061251.1 region 839-2023). The specificity of the probe to the O157 strain was verified using BLAST and PCR techniques.

3. Results and discussion

3.1. DNA immobilization characterization

Fig. 1b depicts a representative shift in the $I_D - V_{GS}$ curves for a typical transistor in the array. In this case, the solid curve corresponds to a 'baseline' measurement prior to exposure to DNA, and the dashed curve was taken after immobilization of the probe DNA on the active area. In each case, the curves were traced by measuring the drain current as a function of the gate voltage applied on the Ag–AgCl electrode in contact with the Top Gate Buffer (TGB, 1 mM TE, pH 8). During immobilization, the chip was exposed to thiol-modified single stranded DNA (45 mer), suspended in TGB as explained in the previous section. The two curves are similar in structure except that DNA probe immobilization has caused a 200 mV positive shift relative to the baseline. The shift can be attributed to the accumulation of charges on the active area of the transistor due to the immobilization of the probe DNA. One can use Eq. (1) to estimate the coverage of the probe DNA on the chip. Starting with the known ionic concentration of the TGB, the Debye length can be calculated using the following equation (Aschenbach, 2011)

$$\lambda_D = \frac{0.31\,\text{nm}}{\sqrt{[c]}} \tag{3}$$

where [c] is the bulk ionic concentration specified in molarity. In this case $c = 1$ mM was used, giving the Debye length of approximately 9.8 nm. Using this into Eq. (2), and using 80 for the dielectric constant for water, the effective capacitance can be estimated and the resulting surface charge density from Eq. (1)

$$\Delta\sigma_{DNA} = \Delta V_{th} \times C_D = \Delta V_{th} \times \varepsilon_{buffer}/\lambda_{Debye} = 0.0145\,\text{C/m}^2$$

Assuming further that the effective number of detectable bases within the Debye length is 10, the probe coverage can be estimated at $(0.0145\,\text{C/m}^2)/(10 \times 1.6 \times 10^{-19}\,\text{C}) = 9 \times 10^{15}\,\text{m}^{-2} = 9 \times 10^{-3}\,\text{nm}^{-2}$. Or equivalently, the average spacing between neighboring probes is approximately 10.5 nm. This coverage is sufficiently low for thiol-modified DNA on gold (Demers et al., 2000), so that no significant steric hindrance is expected and that hybridization efficiency approaching 100% is anticipated.

3.2. Transient signal response from buffer and temperature changes

By necessity, the composition of the buffers as well as the temperature conditions for hybridization and measurements are markedly different. On the one hand, hybridization buffers require free ions to screen the charges of the DNA phosphate backbone. The screening effect reduces the electrostatic repulsion between the single stranded DNA strands to allow them to come into close proximity and initiate the Watson–Crick base-pairing. In this experiment, the hybridization buffer contained 100 mM NaCl dissolved in 1 mM TE. On the other hand, the measurement buffer (TGB) requires low ionic concentration in order to reduce the Debye capacitance sufficiently to produce large voltage shifts from the surface charges as given in Eq. (2).

Moreover, the chip is also subjected to temperature variations from room temperature to 55 °C during hybridization and back to room temperature during measurements. These treatments give rise to transient signal increases the first time that the chip is exposed to hybridization conditions from storage. Fortunately, the transient response quickly diminishes after a couple of consecutive 'blanking' steps. A "Blank" step corresponds to the measurement after the chip was exposed to hybridization conditions albeit without target DNA. A typical result is shown in Fig. 3a. The first blanking step produced as much as 102 mV shift, but by the third blanking step, the system had stabilized to a residual signal well within the experimental noise floor. Based on this, multiple consecutive blanking steps have become part of the testing protocol, and all successive experiments ensured stabilized conditions.

3.3. Signal reduction with repeated measurement

Apart from the effects of buffer and temperature changes, there is also signal decrease with repeated measurement cycles. This effect can be understood based on the following experiment on one representative transistor whose results are plotted in Fig. 3b. After probe immobilization four measurement runs were performed to ensure that stable conditions have been met. The threshold voltage was set as reference. Next, a hybridization with 25 ng/μl complementary target DNA was performed under the usual conditions of temperature and buffer, which was followed by 13 successive measurement repeats on the without changing the buffer and temperature conditions. Then a second hybridization using 50 ng/μl target was performed, and followed by 4 successive measurements. As shown in Fig. 3b both hybridizations caused a rapid spike in the threshold voltage, which gradually decreased with repeated measurements. It was further verified in other experiments that the effect did not depend on time (Aschenbach, 2011). The exact cause for this gradual decrease in V_{th} is still under investigation, but it can be attributed to a drift of the threshold voltage internal to the carbon nanotube transistors from the accumulation of trapped charges on the gate oxide from the applied V_{GS} voltage sweep. Partial dehybridization due to exposure to cycles of V_{GS} may also be a contributing factor. Nevertheless, based on this result, a protocol was established for all successive experiments to use no more than the first 3 measurement cycles after hybridization. To improve the statistics many transistors were included in establishing the average signal shift per run. The transistors were selected using an algorithm that accepts only those devices that fall within an acceptable range of characteristics such as zero hysteresis, leakage current of less than 10 pA and initial threshold voltage less than 1.5 V. Approximately 80% of the transistors were in the acceptable range.

3.4. E. coli detection

3.4.1. Synthetic target DNA

To evaluate the ability of this system to detect *E. coli* DNA, chips were hybridized with highly concentrated synthetic DNA representing part of the gene fragment of the O157 strain. The

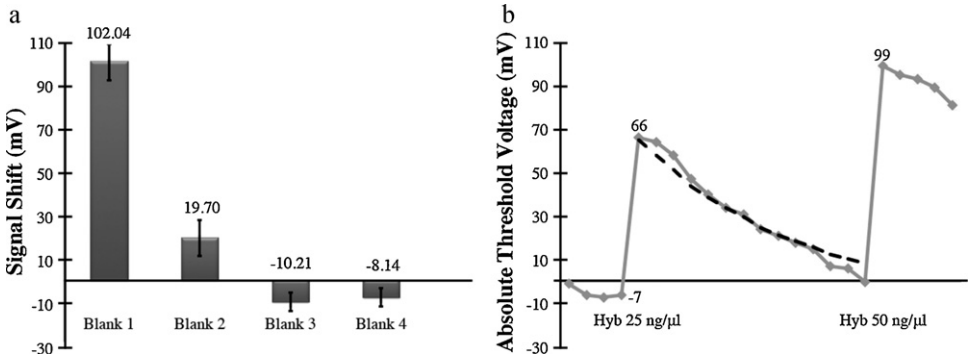

Fig. 3. (a) Successive blanking to achieve equilibrium. (b) Change in absolute V_{th} with repeated trials.

signals were systematically recorded, starting from probe immobilization and on to a series of hybridization and dehybridization steps. The result is summarized in Fig. 4a, which plots the signal shift from each step. The change in threshold voltage relative to the baseline after probe immobilization with 1 mM probe DNA (Post-immobilization) is +113 mV which indicates the effectiveness of probe immobilization using thiol-to-gold chemistry. The first hybridization with a highly concentrated synthetic target DNA (Hyb1) (>1 g/l) produced +147 mV shift, indicating successful capture of the target DNA. The fact that the signal shift is higher than the immobilization step may indicate that some non-specific binding has occurred. The dehybridization (DeHyb1) data was obtained after heating the chip to 95 °C, just a few degrees higher than the probe's melting temperature while replacing the buffer solution. The buffer was replaced three times. This yielded a −63 mV signal shift, which indicates that target and probe have denatured and the target DNA was washed off the chip. Two additional steps of hybridization and dehybridization were performed which produced +105 mV (Hyb2) and +71 mV (Hyb3) shifts, respectively while the dehybridizations yielded −55 mV (DeHyb2) and +10 mV (DeHyb3), respectively. These results are consistent with negative charge accumulation on the gold gate surface for probe immobilization and hybridization, which in turn was measurable as a positive shift in V_{th}, while the dehybridization reduced the surface charges. One could further infer from the overall decrease in the magnitude of the signal shifts with repeated steps that the dehybridization procedure may not have completely removed the bound target DNA, to the extent that the probe sites may have been saturated after the third cycle.

To access the performance of the chip with relatively lower target concentrations, a similar experiment was repeated on another chip with 100 fold less DNA. But, instead of the dehybridization step, the hybridizations were interleaved with 'Blanks'. 'Blank', as explained earlier are identical to hybridization conditions but without the target DNA. This step is also important to ensure that no threshold shift occurs in the absence of target hybridization. The results are presented in Fig. 4b showing the cumulative effect of target loading by successively increasing concentrations of target DNA. As listed in Fig. 4c there is a nearly linear increase in the cumulative voltage per decade increase in concentration from 0.014 g/l to 1.4 g/l. The lesser differential increment of 113.74 mV between 0.14 g/l and 1.4 g/l compared with the 139 mV shift between 0.014 g/l and 0.14 g/l may be explained by the possible saturation of the probe sites by the target DNA.

3.4.2. Highly purified genomic target DNA

A typical result for genomic DNA is shown in Fig. 5a which demonstrates the ability of the chip to detect highly purified genomic DNA. Purified genomic target was hybridized under the same conditions of temperature, buffer and time as mentioned in the DNA hybridization protocol in the materials and methods section. The blanking step was performed before hybridizations

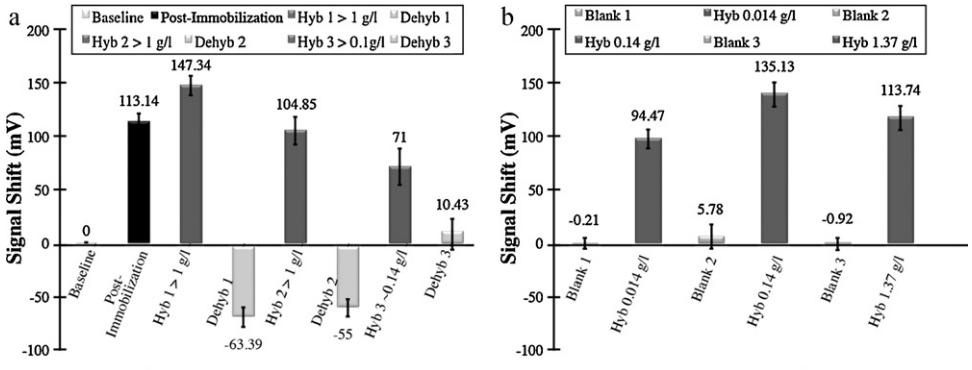

c

Concentration (g/l)	Signal Shift (mV) (Cumulative)
0.014	94.47 (94.47)
0.14	139.13 (233.60)
1.37	113.74 (347.34)

Fig. 4. Results on hybridization with synthetic target DNA. (a) Threshold voltage shift with hybridization/dehybridization sequence on highly concentrated targets (chip W234). (b) Threshold voltage shift with sequential hybridization with progressively increasing target DNA concentration (chip W395). (c) Table showing shifts in signal versus amount of synthetic nucleotide target (chip W395).

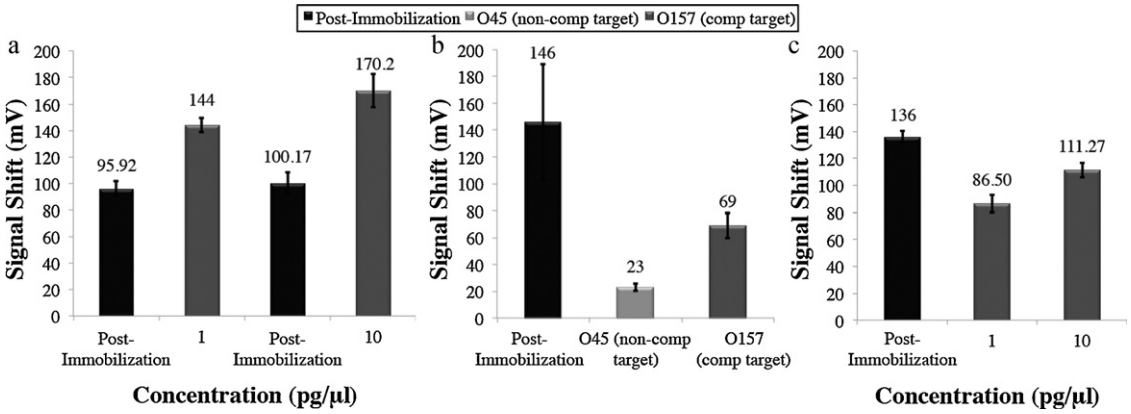

Fig. 5. Results on hybridization with genomic target DNA. (a) Threshold voltage shifts due to hybridization with two concentrations of high purity target DNA (1 pg/μl on chip W391; 10 pg/μl on chip W287). The probe immobilization signal is 95.92 ± 5.58 mV for the 1 pg/μl concentration while it is 100.17 ± 8.34 mV for the 10 pg/μl concentration. (b) Threshold voltage shift comparison between when hybridized with a non-complementary target DNA (negative control *E. coli* 045) and complementary target DNA (*E. coli* 0157). (c) Threshold voltage shifts due to hybridization with two concentrations of crude target DNA (chip W364). The probe immobilization signal is 136 ± 4.3 mV for this chip.

to ensure that the chips are stable and any background signal shifts associated with the hybridization buffer are eliminated. The genomic target DNA at a concentration of 1 pg/μl yielded a shift of +87 mV and at a 10 pg/μl concentration yielded a shift of +111 mV. These sensitivity values are more than 10^5 higher than for short strands of synthetic DNA target. It is fortuitous that the sensitivity is higher for long strands of genomic DNA as compared with short synthetic oligomer targets. This is presumably because of the formation of secondary and other higher order structures on the long target strands that increase the density of the DNA so that more charges are detected within the Debye length.

As different chips were used for each of the hybridizations, there is no question of saturation or unavailability of probe binding sites. The linear increase in shift in V_{th} for a decade increase in the concentration of target DNA, as seen in Fig. 5a, reaffirms that the reuse of the same chip for successive hybridizations without performing the dehybridization step may lead to slightly lower signals due to the unavailability of all probe sites for the target DNA to bind to.

3.4.3. Negative control

To establish that the observed shifts were due to specific detection of *E. coli* O157, a comparison of signal shifts between hybridization using genomic DNA extracted from *E. coli* O45 and *E. coli* O157 at the same concentration (6 ng/μl) was performed under the same aforementioned hybridization conditions. The transistors were immobilized with DNA probe specific to *E. coli* O157 (post-immobilization +146 mV shift). The results is shown in Fig. 5b. As expected there was a slight signal shift detected with *E. coli* O45 due to the non-complementary target. But the signal shift generated was within the noise floor of 20 mV. To further validate that the chip was active, the step was followed by a hybridization using the *E. coli* O157 highly purified genomic target DNA at the same concentration which generated a shift of +69 mV (Fig. 5b). This step provides an additional proof of validity of the probes, protocols and function of the sensor chips.

3.4.4. Crude target DNA

To assess the performance of the system under restrictive sample preparation conditions, two successive sensing steps were performed on DNA extracted from *E. coli* O157 using simple boiling method. DNA extracted using such a method mimics DNA samples collected in the field. After the threshold voltage was stabilized from the blanking steps, the first hybridization was performed with 1 pg/μl concentration of the target DNA, which produced +144 mV shift. A second hybridization with a ten-fold increase in concentration of the DNA target resulted in +170 mV. These results shown in Fig. 5c are very similar to those obtained for highly purified DNA, which suggests the utility of the technique for use in crudely extracted DNA.

The results in this section show the successful detection of *E. coli* O157 in the form of single stranded 45-mer synthetic DNA target, highly purified genomic DNA target and crude genomic DNA target extracted by the boiling method. Higher signal shifts were observed with the genomic DNA (both crude and highly purified) as compared to the synthetic DNA targets. In fact, a concentration of about 1,000,000× is needed for synthetic DNA to achieve the same signal as the genomic DNA. This could be due two reasons: First, the length of the genomic DNA targets is much larger (a few kilo bases) as compared to the single stranded synthetic DNA target which is only 45 mer long (Table 1). Hence more charge is deposited on the active region when the target is genomic DNA; secondly, the long genomic DNA may form secondary loop structures such that a large number of oligonucleotides fall within a distance of λ_{Debye} (Debye length) from the surface of the active region. Both these can contribute to much higher charge accumulation from genomic DNA and hence result in larger signal shifts as compared to the synthetic targets.

It is worth noting that hybridization with PCR products was also performed but yielded inconsistent results. Presumably the presence of ions in the PCR reaction mix and other free ionic charges adhere indiscriminately to the active areas.

4. Conclusion

A new and highly sensitive platform has been developed for the detection of *E. coli* O157. Target DNA concentration of as low as 1 pg/μl was successfully detected using the biosensor chip. The chips can detect target DNA extracted using simple boiling method with equal sensitivity of highly purified DNA. Moreover, the crude target DNA sample used for hybridization required a limited pre-enrichment step thereby offers potential in significantly reducing the time for detection. A negative control was performed which resulted in almost no shift in signal compared with the background noise indicating the resistance to false positive conclusions. The ability of this method to detect a low level of crude DNA suggest its potential to be used in the field with minimal pre-enrichment.

References

Associated Press, 2011. http://www.ap.org/.

Aschenbach, K.H., 2011. Development of carbon nanotube field-effect transistor arrays for detection of Her2 overexpression in breast cancer. Ph.D. Thesis.
Beran, G.W., et al., 1991. Dairy Food Environ. Sanit. 11, 189–194.
Buchanan, R.L., Doly, M.P., 1997. Food Technol. 51, 69–76.
Demers, L.M., et al., 2000. Anal. Chem. 72, 5535–5541.
Griffin, P.M., Tauxe, R.V., 1991. Epidemiol. Rev. 13, 60–98.
Helrich, K., 1990. Official Methods of Analysis of the Association of Official Analytical Chemists, Microbiological Methods, vol. 2, 15 edn. AOAC, Arlington, VA, pp. 425–497 (Chapter 17).
Hobson, N.S., et al., 1996. Biosens. Bioelectron. 11 (5), 455–477.
Ivnitski, D., et al., 1999. Biosens. Bioelectron., 14.
Jaeger, J.L., Acheson, D.W., 2000. Curr. Infect. Dis. Rep. 2, 61–67.
Karch, H., et al., 1999. Diagn. Microbiol. Infect. Dis. 34, 229–243.
Kaspar, C.W., Tartera, C., 1990. Methods Microbiol. 22, 497–530.
Liu, Y., Fratamico, P., 2006. Mol. Cell. Probes.
Maehashi, K., et al., 2004. Jpn. J. Appl. Phys.
Meng, J.H., et al., 1996. Int. J. Food Microbiol. 32 (1–2), 103–113.
Pandana, H., et al., 2008. IEEE Sens. J.
Potter, M.E., et al., 1997. In: Doyle, M.P., Beuchat, L.R., Montville, T.J. (Eds.), Food Microbiology: Fundamentals and Frontiers. Washington, DC, ASM Press.
Quadri, S.M., Kayali, S., 1998. Postgrad. Med. 103, 179–180.
Samuel, G., Reeves, P., 2003. Carbohydr. Res.
Sperveslage, J., et al., 1996. J. Microbiol. Methods 26 (3), 219–224.
Star, A., et al., 2007. Adv. Mater.
Tietjen, M., Fung, D.Y.C., 1995. Crit. Rev. Microb. 21, 53–83.